

An automatic fundus image analysis system for clinical diagnosis of glaucoma

Chih-Yin Ho¹ and Tun-Wen Pai^{1,*}

¹Department of Computer Science and Engineering,
National Taiwan Ocean University, Keelung, Taiwan
*twp@mail.ntou.edu.tw

Hao-Teng Chang² and Hsin-Yi Chen³

²Graduate Institute of Molecular Systems Biomedicine,
³Department of Ophthalmology, China Medical
University and Hospital, Taichung, Taiwan

Abstract—Glaucoma is a serious ocular disease and leads blindness if it couldn't be detected and treated in proper way. The diagnostic criteria for glaucoma include intraocular pressure measurement, optic nerve head evaluation, retinal nerve fiber layer and visual field defect. The observation of optic nerve head, cup to disc ratio and neural rim configuration are important for early detecting glaucoma in clinical practice. However, the broad range of cup to disc ratio is difficult to identify early changes of optic nerve head, and different ethnic groups possess various features in optic nerve head structures. Hence, it is still important to develop various detection techniques to assist clinicians to diagnose glaucoma at early stages. In this study, we developed an automatic detection system which contains two major phases: the first phase performs a series modules of digital fundus retinal image analysis including vessel detection, vessel inpainting, cup to disc ratio calculation, and neuro-retinal rim for ISNT rule; the second phase determines the abnormal status of retinal blood vessels from different aspect of view. In this study, the novel idea of integrating image inpainting and active contour model techniques successfully assisted the correct identification of cup and disk regions. Several clinical fundus retinal images containing normal and glaucoma images were applied to the proposed system for demonstration.

Keywords- fundus retinal image; glaucoma; vessel inpainting; vessel detection; cup to disc ratio; ISNT rule.

I. INTRODUCTION

New statistics reported by WHO have shown that glaucoma is now the second leading cause of blindness globally, and it is estimated to be responsible for 12 percent of global blindness [1]. A research report published by British Journal of Ophthalmology pointed out that the global toll of the disabling eye causing by glaucoma is reaching to 60.5 million by 2010, and rising to almost 80 million by 2020. Especially, women and people living in Asia, Africa, and India will be most badly affected [2]. Hence, a timely and precise early detection of glaucoma plays a key role for preventing irreversible damages in eyes.

Three structural anatomical elements can be observed in the rear pole of the retina fundus image including macula, optic disc (optic nerve head), and the vascular network. The vascular network is composed of the thicker veins with darker red and the thinner arteries with lighter reddish tone. A cup is presented as an empty space in the middle part of

the optic disk surrounded by optic nerve fibers. With the loss of nerve fibers from glaucoma attack, the cup area becomes larger gradually because of less space occupied by remaining nerve fibers. A healthy optic nerve possesses abundant nerve fibers traveling through it (approximately 1.2 million fibers [3]), and it is usually appeared as a small cup. Hence, the proportion of a cup diameter with respect to its optic disk diameter is often described by the ophthalmologist and named as a “cup to disc ratio”. Due to uncertain borders and subjective perceptions, quantitative calculation of cup to disk ratios during routine examination of a patient is not easy to be consistent, and it leads to uncertain diagnosis results even identified by experienced ophthalmologists [4]. Thus, an intuitive, efficient and objective method for automatically classifying digital fundus images into either normal or glaucomatous types is urgently required for facilitating ophthalmologists. In this study, we designed an auxiliary diagnosis system which can automatically calculate and analyze the cup to disc ratio, neuro-retinal rim configuration, abnormal retinal nerve fibers, and the extraordinary retina blood vessels to assist glaucoma diagnosis in a consistent way.

II. PROPOSED METHOD AND FLOWCHART

In this system, the measurement of cup to disc ratio, neuro-retinal rim configuration and vessel distribution information are considered as important features, and they are extracted and evaluated through the designed sequential modules automatically. The initial step is to detect vasculars by two structural characteristics : shape and continuity features. Subsequently, regions of identified vasculars are removed and compensated by employing FMM inpainting method to cover a vessel-free image prior to the optic disk extraction. Next, local peak thresholding analysis from histogram of an inpainted image is performed for region segmentation and each image will be segmented into three major regions. Three segmented regions are circularly fitted with two circles to obtain initial boundaries within the optic disc regions. Then, the active contour model algorithm is applied to detect the true boundaries of inner cup and surrounding disk. Finally, the cup to disc ratio parameter is calculated by taking the ratio between diameters of detected optic cup and disc, and the inferior, superior, nasal and temporal margin widths is also estimated for diagnosis.

Figure 1 depicts the five major modules for building the proposed detection system, which include vessel detection, vessel inpainting, optic disk boundary detection, cup to disk ratio analysis and ISNT rule analysis. Each module is described in the following sections.

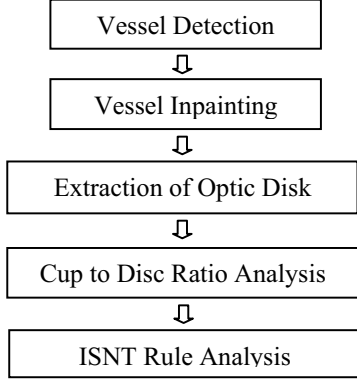


Figure 1. System flowchart of the proposed glaucoma detection system.

III. VESSEL DETECTION

A. Vessel Detection

Three anatomical elements are observed from a fundus image including macula, the optic disk, and the vascular network (composed of nerve-fibers and vessels). Some of the vascular networks appear within the optic disk which influence the detection of borders and affect the accurate calculation of cup to disk ratios. Hence, it is helpful if the vessels can be detected, removed, and accurately inpainted prior to the cup to disk ratio calculation. The proposed system adopted two important features of shape and continuity for vascular detection [5], and the corresponding formula with respect to various conditions and probabilities were established correspondingly. At the first step of vessel detection, a Canny edge detection method is applied to detect general edges within a query fundus image. Here, only the green channel subimage from the original image was used for analysis due to its high contrast compared to the red and blue channel subimages. The detected contours by Canny algorithms contained boundaries of blood vessels and some other macula noise. All retrieved segments were then re-verified based on shape and continuity features of vascular elements for blood vessel identification.

A.1 Shape

The boundaries of a vascular segment are assumed in parallel and close to each other with a perpendicular direction. Under this concept, we can take two adjacent edge points P_i and P_j on row r from the detected edge map. If both P_i and P_j satisfy the Equation (1) and (2) simultaneously, the connected line from P_i to P_j can be defined as a cross section of a vessel. In order to establish the probability of each cross section, the Equation (3)

defines a confidence value C_l for improvement. The confidence values of non-vessel pixels (not located on cross sections) are set as 0.

$$(P_i - P_j) > D_l \text{ or } (P_i - P_j) < D_h \quad (1)$$

$$\mu(\gamma, P_i, P_j) < \mu(\gamma, P_i - D_l, P_i - 1) \text{ and}$$

$$\mu(\gamma, P_i, P_j) < \mu(\gamma, P_j + 1, P_j + D_l) \quad (2)$$

$$C_l = (E_i + E_j) e^{-\alpha_l |E_i - E_j|} \quad (3)$$

In the experiment, D_l is the minimum distance from P_i to P_j and set as 2, and D_h is the maximum distance from and set as 25; $\mu(\gamma, P_i, P_j)$ denotes the mean value of image intensity from P_i to P_j in row r within the green channel subimage; D_l is defined as the neighbor pixels at each side and set as 5; E_i and E_j represent the intensities of P_i and P_j respectively; α_l is set as 0.05 for an adjustable parameter. Accordingly, a confidence map S_h can be established for horizontal direction of vessel features. Similarly, the confidence map S_v is also constructed for vertical direction. Both maps S_h and S_v are considered as the shape characteristics for vessel detection.

B. Continuity

The previous shape feature alone is not satisfied for accurate vessel detection. By observation, blood vessels often possess extended linear and continuous structures. If one cross section and the other cross section are neighborly connected and possess similar features, they can be considered as continuing cross segments. More specifically, one cross section $[P_i, P_j]$ is defined at row r with the horizontal direction and another cross section $[P_i', P_j']$ is found at row $r+1$. Both sections can be recognized as a continuous cross segment when both segments satisfy the conditions described in Equation (4) and (5). The cross sections can therefore be divided into different groups due to distantly geometrical locations and/or inconsistent neighboring properties, and the extracted cross segments can be regarded as the same blood vessel while satisfying both conditions of continuous structural characteristics.

Condition 1: two horizontal cross sections overlapped in vertical direction, or two vertical cross sections overlapped in the horizontal sections. (4)

Condition 2: length difference between two neighboring cross sections must be less than a thresholding value λ (set as 5 in this study). (5)

According to the examined conditions, the confidence value C_2 of each cross segment is calculated by Equation (6). Based on the confidence values, a confidence map C_h can be obtained with respect to the horizontal direction, and C_v for vertical direction. Both maps C_h and C_v are established by adopting the continuity characteristics for vessel detection.

$$C_2 = e^{-\alpha_2 * \sigma \ln(L)} \quad (6)$$

where L is the number of cross section; σ is defined as the width variance of cross section within a cross segment; α_2 is defined as a positive weighting factor and set as 0.3 as a default value in this study.

C. Confidence Map

Adopting previous two characteristics of blood vessels, four maps (S_h, S_v, C_h, C_v) containing confidence values are further evaluated for vessel detection. Here, the Bayesian formula in Equation (7) is illustrated for processing horizontal confidence maps. If S_h and C_h are assumed independent for each other and the $P(\text{Vessel})$ is considered to be uniformly distributed, the Equation (7) can be simplified and re-written as in Equation (8). With similar assumptions for vertical confidence maps, two new images can be formulated as the confidence maps M_h and M_v , and the definition of a final confidence map is constructed by taking $M = \max(M_h, M_v)$.

$$P(\text{Vessel} | S_h, C_h) = P(\text{Vessel})P(S_h, C_h | \text{Vessel}) / P(S_h, C_h) \quad (7)$$

$$P(\text{Vessel} | S_h, C_h) \propto P(S_h | \text{Vessel})P(C_h | \text{Vessel}) \quad (8)$$

The complete vessel detection flow chart is described as follows. The selected green channel from an input fundus image provides a clearer resource for Canny edge detection[6][7]. Combining both horizontal and vertical confidence maps regarding to shape and continuity features generates an accurate confidence map by Bayesian rules. Once a final confidence map is obtained, the system performs morphological filters for removing isolated noise and smoothing the obtained vascular objects. In Figure 2, the output of each module designed in the proposed system for detecting vessels from a fundus image is demonstrated for its applicability.

IV. INPAINTING MODULE

The inpainting algorithm is designed for rebuilding missing regions within a deteriorated image. In this paper, an inpainting module is applied to fill up the blank regions after removing detected vessels in the previous procedures. Here, the FMM (Fast Marching Method) [8] was adopted to accomplish the inpainting function due to its efficiencies and effectiveness. The proposed method fills blank regions from outer areas to central parts progressively according to the graylevels of known image pixels close to the target regions. In this study, a first order approximation was applied to the originally known image areas with a normalized weighting function, the detail algorithms are described in the following sections.

A. FMM

The idea of FMM inpainting module is depicted in Figure 3. A point p is located on the boundary $\partial\Omega$ of the region Ω which is the target region to be inpainted. In order to decide the graylevel of point p , a small circle neighborhood $B_\varepsilon(p)$ of radius ε is defined by taking pixel p as the center. For the Equation (8), it applies the first order approximation for inpainting point p within the region $B_\varepsilon(p)$ by calculating the contribution from the image level of $I(q)$ and gradient value $\nabla I(q)$ regarding the point q . Then, it sums up the contribution from all points within the $B_\varepsilon(p)$ to

inpaint p by incorporating weighting function $w(p, q)$ described in Equation(10).

$$I_q(p) = I(q) + \nabla I(q)(p - q) \quad (9)$$

$$I(p) = \frac{\sum_{q \in B_\varepsilon(p)} w(p, q)[I(q) + \nabla I(q)(p - q)]}{\sum_{q \in B_\varepsilon(p)} w(p, q)} \quad (10)$$

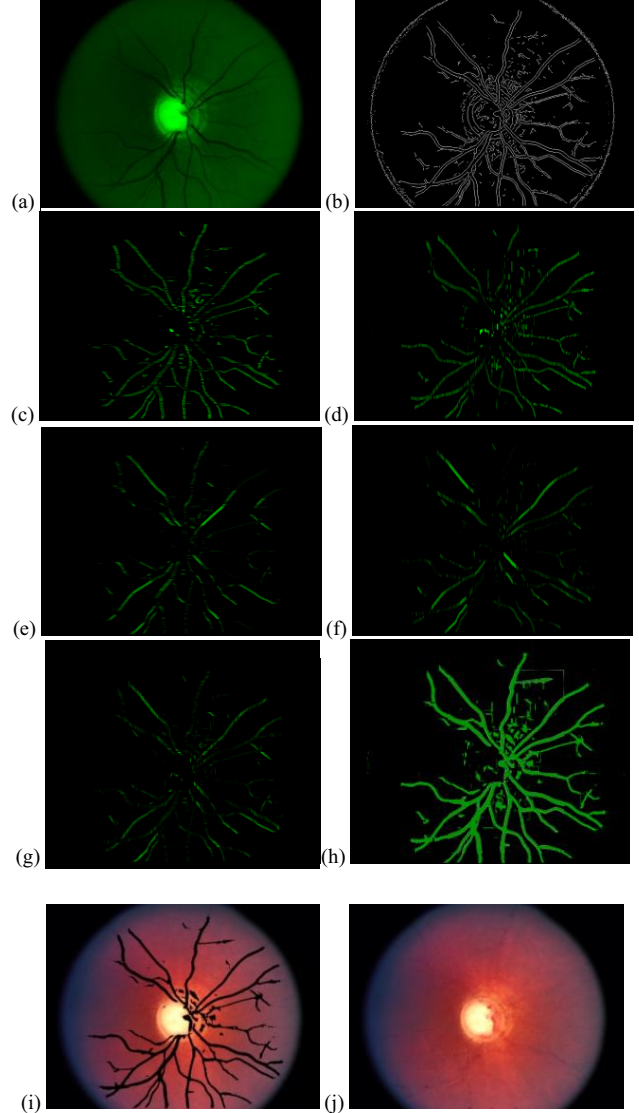


Figure 2. (a) The green subimage from an input fundus image, (b) detected Canny edges, (c) shape confidence map in horizontal direction, (d) shape confidence map in vertical direction, (e) continuity confidence map in horizontal direction, (f) continuity confidence map in vertical direction, (g) final confidence map through Bayesian detection, (h) after morphological filtering processing, (i) detected vessel segments within the original fundus image, and (j) inpainted fundus image.

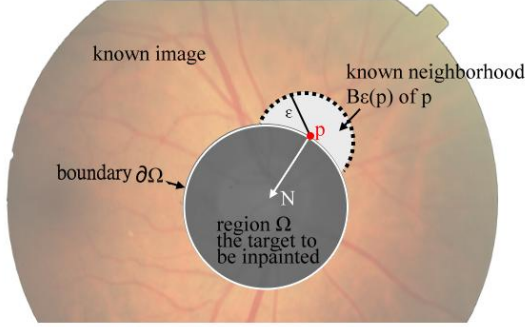


Figure 3. The FMM inpainting principle

To inpaint all points in target region Ω , Equation (10) is applied to all the points on the boundary $\partial\Omega$, and the distance is increased from boundary $\partial\Omega$ to the internal positions of Ω . FMM ensures the nearest points located on the boundary $\partial\Omega$ possessing a higher priority to be inpainted, and it is executed until all the target region Ω is patched. A weighting function $w(p, q)$ is applied to propagate the gray value as well as the sharp details of $B_\epsilon(p)$, and it is defined as $w(p, q) = \text{dir}(p, q) \cdot \text{dst}(p, q) \cdot \text{lev}(p, q)$ and formulated in Equations (11), (12), and (13).

$$\text{dir}(p, q) = \frac{p - q}{\|p - q\|} \cdot N(p) \quad (11)$$

$$\text{dst}(p, q) = \frac{d_0^2}{\|p - q\|^2} \quad (12)$$

$$\text{lev}(p, q) = \frac{T_0}{1 + |T(p) - T(q)|} \quad (13)$$

Equation (11) describes the directional component $\text{dir}(p, q)$ which ensures the contribution of pixels closed to the normal direction $N = \nabla T$ more than the pixel distance from direction N . Equation (12) of $\text{dst}(p, q)$ defines the geometric distance component, which describes pixels near p providing more contribution during inpainting processes. Equation (13) described the level set distance component, $\text{lev}(p, q)$, that ensures pixels closed to the contour through point p possessing more contribution than other pixels. Based on calculating these inpainting parameters, a smooth and accurate filling result can be obtained for facilitating the following optic disk detection. An inpainted fundus image is shown in Figure 2(j).

V. EXTRACTION OF OPTIC DISK

To precisely define the optic cup and disc areas is the main goal for glaucoma diagnosis in this study. After the vessel inpainting processes, the system performs the module of optic disk analysis to extract the regions within the retinal fundus image which contains the optic disc. Based on the observation from obtained clinical fundus images, the cup and disc areas are brighter and possess higher intensity values than the background image. According to this

assumption, the pixels with higher intensities and ranked within 0.5% from a fundus image are selected as potential candidates for the optic disc regions, and all the identified connected blocks with size larger than certain thresholding value are remained for analysis through a size filtering process. To obtain the target optic disk, a region growing algorithm is performed by taking the largest block as the initial seed, and a heuristic assumption of 1% of the maximum intensity is assigned for thresholding limitations. Thus, a major area can be obtained by applying region growing techniques and an extended version of a square bounding box covering the grown areas is applied for the major segmented areas of optic disk. An example of detected optic disc regions with bounding box information from an original fundus image is shown in Figure 4.

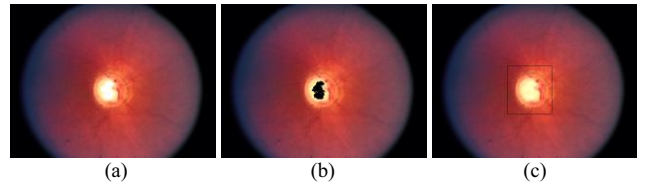


Figure 4. (a) An original fundus image, (b) initial seeds for region growing algorithms, (c) Detected optic disk regions.

VI. CUP AND DISC DETECTION

There are many features for diagnosing glaucoma diseases. The most intuitive features are the cup to disc ratio (CDR) and the change in the cup areas. Due to the influence of glaucoma, the cup areas are increased due to intra ocular pressure and result in dramatic visual loss. The CDR represents the ratio of the diameters of the cup to disc. In this detection system, the proposed module detects the circular boundaries of optic disk and cup regarding to the vessel-free optic disk image, and the diameters and the areas of optic disk and cup can then be calculated automatically. The details of cup and disk detection are described in the following sections.

A. Cup and Disc Region Detection

In order to differentiate the cup and disc regions within the vessel-free and inpainted optic disk image, we analyze the histogram distribution from the previously extracted optic image [9]. For an extracted optimal optic image, there should be three different regions with different intensity levels from light to dark gradually, and represent the areas of cup, disc, and background respectively. To avoid the noisy factors, both the lightest and darkest intensities are initially considered as noisy pixels in this module. Therefore, only pixels with intensity values from 50 to 205 are considered as the target graylevels for cup, disc, and background regions. For a better illustration of the distribution of the optic disc, an example of histogram distribution is shown in Figure 5 by its reversed version, and thus the problem is transferred to detect three major peaks

and corresponding regions. To identify the main peaks from the extracted image, the morphological erosion and dilation operations were implemented for peak extraction. The difference between the eroded and dilated histogram distribution was applied for peak extraction from a reversed histogram. Thus, the two local valleys in the original histogram can be identified and divided the histogram distribution into three main parts respectively. For easy observation, these separated graylevels are displayed in red, green, and blue for a pseudo-color image. Due to the ambiguous distribution of graylevels among the neighboring areas, these three segmented regions are not as smooth as expectation. Therefore, the pixels located on boundary between two neighboring segments are re-verified by considering the slope variations of connective neighboring pairs. If the slope variation is large compared to two neighboring pairs, they are not considered as boundary pixels. Once the boundary pixels are detected, a module of circle curve fitting procedures is applied to define optimal circles of the boundary pixel sets. Accordingly, two optimal circles were obtained for the following cup to disc ratio analyses.

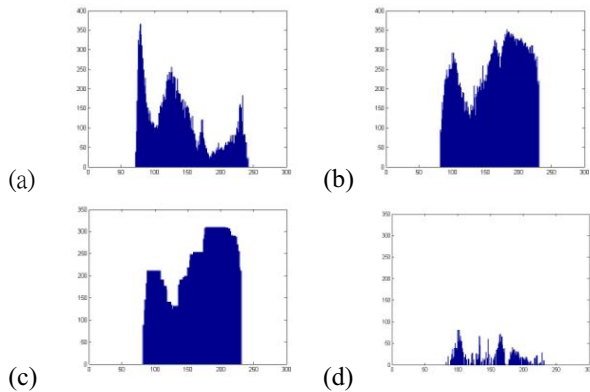


Figure 5. (a) Histogram of an optic disc image, (b) reverse histogram(after trimming extreme values on both ends), (c). Eroded and dilated results of (b), (d) difference between (b) and (c).

B. Active Contour Model

Active contour model (ACM), also called snake algorithms, was introduced by Kass et al. in 1987[10]. ACM is a framework for delineating borders of objects within a possibly noisy image, and which has been successfully used in contour detection for different applications. ACM is a dynamic model as it always iteratively minimizes its total energy defined as the sum of internal and external energy. However, the result by ACM approach is very sensitive to the positions of initial contours. Hence, it is crucial to provide the initial contours obtained from previous steps. Here, the two optimal fitted circles are selected as the initial contours for further detection of non-circular cup and disk in general condition.

C. Cup to Disc Ratio

The cup to disc ratio (CDR) is one of the most important

factors for the diagnosis of glaucoma since a higher contrast between the cup and disc regions is expected. Here, the CDR parameter is measured by considering the horizontal diameters of the cup and disc regions. When the CDR is greater than a value of 0.6, the patient is diagnosed as glaucoma, and a normal condition for CDR is less than or equal to 0.4. Two of the conditions will be diagnosed as glaucoma suspect: 1) inter-eye asymmetry of CDR of 0.2 or above ; 2) CDR between 0.4 and 0.6. However, some of the fundus image will be identified as glaucoma through the vessel distribution analysis at previous vessel detection stages.

D. ISNT Rule Analysis

With the precise information of cup and disk boundaries, the neural rim configuration becomes available for the diagnosis of glaucoma according to the ISNT rule [11-14]. For a normal optic disk, the neural rim follows the property of decreasing thickness in an order of inferior, superior, nasal and temporal rims, *i.e.* the inferior neuro-retinal rim possesses the thickest portion and the temporal rim is the skinniest portion. Glaucoma frequently damages superior and inferior optic nerve fibers before temporal and nasal fibers, and it leads to decrease the superior and inferior rims and change the order of ISNT relationship. Hence, the detection of rim distances in four directions can assist the correct verification of ISNT rule and then improve the correct diagnosis of glaucoma at early stages.

VII. VESSEL EMBLEMED IMAGE

Sometimes the boundaries of cup and disk are not easy to detect accurately, especially for different types of glaucoma. Hence, in addition to cup and disk analysis for glaucoma detection, the extracted vessels from previous "vessel detection" steps can also be considered as auxiliary diagnosis. The abnormal retinal vessels from patients are also important factors and indicators that could lead to glaucoma such as vascular thickening, distortion, vessel hemorrhage, retinal vascular occlusion, and abnormal angiogenesis. Hence, the determination of abnormal appearance of vessels is proposed for additional diagnosis of glaucoma. For example, both a normal vessel and a vessel hemorrhage cases are displayed in Figure 6 for comparison. The irregular growth of detected blood vessels and shown as blocked vessel objects can be diagnosed as a hemorrhage glaucoma without using cup to disk ratio parameter.

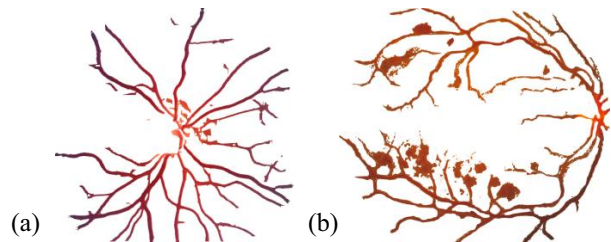


Figure 6. Vessel extracted images : (a) normal vessel; (b) vessel hemorrhage.

VIII. RESULTS AND DISCUSSIONS

We designed an automatic glaucoma detection system through vessel detection, CDR parameter calculation and ISNT rule analysis, which facilitates early diagnosis of glaucoma and follow-up evaluation. Two examples are illustrated in Figure 7 for assessing the validity of our proposed method. More chronic data will be collected (from Chinese Medical University Hospital, Taiwan) and carefully evaluated under regular follow-up diagnosis, and the results will be reported soon. Although the proposed method is not an error-free system, the pioneering testing results indicate that the proposed algorithms can be used as an auxiliary tool by ophthalmologists for cross verification. In Figure 7, the first row is an example of glaucoma and it was correctly detected since both the cup to disk ratio and the violated ISNT rules were identified. The second row is a normal case and it was correctly detected as a normal condition. Though the cup to disk ratio is located within a suspect range, the ISNT rule was re-verified as a normal condition. In fact, a set of testing examples were predicted in wrong results during system evaluation. Most of testing samples with wrong prediction were due to no clear optic cup on the vessel-free images, neither could be observed by human eyes directly. For some of the cases, the initial cup and disc boundaries were overlapped by virtual circles, and therefore, wrong ACM contours were obtained and lead to wrong CDR parameters and ISNT rims for detection. It was happened mainly due to the developed system cannot adaptively select a suitable graylevel for each fundus image, and error results were made by wrong identified optic disc boundaries. Maybe a dynamic histogram equalization technique for fundus images can be designed for enhancing the image contrast, and we believe that the accuracy of the proposed methods can be tremendously improved.

References

- [1] WHO: <http://www.who.int/blindness/causes/priority/en/index7.html>, accessed Jan. 2011.
- [2] H A Quigley, A T Broman, "The number of people with glaucoma worldwide in 2010 and 2020," *British J. Ophthalmology* 90, 262–267, 2006.
- [3] DOUGLAS J. RHEE, M.D., "Optic Neuropathy with Pathological Cupping" *Massachusetts Eye and Ear Infirmary, Department of Ophthalmology, Boston, Massachusetts*, 2006.
- [4] Kanski J. et al. "Glaucoma: a color manual of diagnosis and treatment." *Butterworth-Heinemann*, 1996.
- [5] K. Huang and M. Yan, "A region based algorithm for vessel detection in retinal images," *Med Image Comput Comput Assist Interv*, vol. 9, pp. 645-53, 2006.
- [6] Stall, J., Abramoff, M., et al, "Ridge-based vessel segmentation in color images of the retina," *IEEE Transactions on, Medical Imaging*, vol. 23, No. 4, Apr 2004.
- [7] J. Canny, "A Computational Approach to Edge Detection," *Pattern Analysis and Machine Intelligence, IEEE Transactions on*, vol. PAMI-8, pp. 679-698, 1986.
- [8] Alexandru Telea, "An Image Inpainting Technique Based on the Fast Marching Method," *Eindhoven University of Technology*, Vol. 9, No. 1: 25–36.
- [9] Hao-Teng Chang, Chih-Hong Liub and Tun-Wen Paib "Estimation and extraction of B-cell linear epitopes predicted by mathematical morphology approaches," *Published online in Wiley InterScience*: 2008.
- [10] M. Kass, A. Witkin, and D. Terzopoulos, "Snakes - Active Contour Models," *International Journal of Computer Vision*, 321-331, 1987.
- [11] Harizman N, Oliveira C, Chiang A, et al, "The ISNT rule and differentiation of normal from glaucomatous eyes," *Arch Ophthalmol*, 124:1579–583, 2006.
- [12] Fingeret M, Medeiros FA, Susanna R, Weinreb R, "Five rules to evaluate the optic disc and retinal nerve fiber layer for glaucoma," *Optometry*, 76:661–668, 2005.
- [13] Jonas JB, Gusek GC, Naumann GOH, "Optic disc, cup and neuroretinal rim size, configuration and correlations in normal eyes," *Invest Ophthalmol Vis Sci*, 29:1151–1158, 1988.
- [14] Jonas JB, Fernández MC, Stürmer J. Pattern of glaucomatous neuroretinal rim loss," *Ophthalmology*, 100:63–68, 1993.


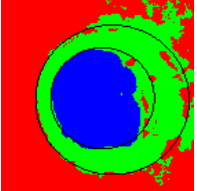

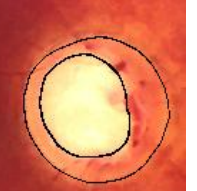
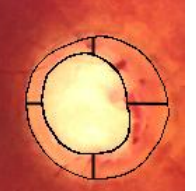

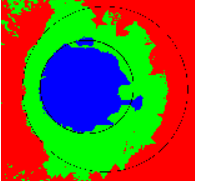
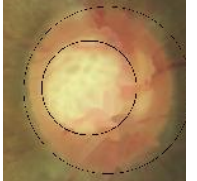


Fundus retinal image	Extracted and segmented regions with fitted circles	Detected cup and disc regions (without vessels)	Cup and disk boundaries after ACM detection	ISNT analysis	Diagnosis Results
					<p>Glaucoma</p> <p>CDR(circle)=0.68 Horizontal CDR(ACM)=0.60 Vertical CDR(ACM)=0.68 I:0.15 S:0.13 N:0.28 T:0.11 Violate ISNT rules</p>
					<p>Normal</p> <p>CDR(circle)= 0.56 Horizontal CDR(ACM)=0.68 Vertical CDR(ACM)=0.54 I:0.27 S:0.18 N:0.16 T:0.12 Obey ISNT rules</p>

Figure 7. Serial output images obtained from the proposed system and corresponding parameters for glaucoma detection.